

# Designer thermal switches: Effect of the contact material on instantaneous thermoelectric transport through a strongly interacting quantum dot

A. Goker<sup>1</sup> and E. Gedik<sup>2</sup>

<sup>1</sup> *Department of Physics,  
Bilecik University,  
11210, Gölümbe, Bilecik, Turkey and*

<sup>2</sup> *Department of Physics,  
Eskisehir Osmangazi University,  
26480, Meselik, Eskisehir, Turkey*

(Dated: September 29, 2018)

We investigate the effect of contact geometry on the instantaneous thermoelectric response of a quantum dot pushed suddenly into the Kondo regime via a gate voltage using time dependent non-crossing approximation and linear response Onsager relations. We utilize graphene and metal contacts for this purpose. Instantaneous thermopower displays sinusoidal oscillations whose frequency is proportional to the energy separation between the van Hove singularity in the contact density of states and Fermi level for both cases regardless of the asymmetry factor at the onset of Kondo timescale. The amplitude of the oscillations increases with decreasing temperature saturating around the Kondo temperature. We also calculate the instantaneous figure of merit and show that the oscillations taking place at temperatures above the Kondo temperature are enhanced more than the ones occurring at lower temperatures due to the violation of the Wiedemann-Franz law. Graphene emerges as a more promising electrode candidate than ordinary metals in single electron devices since it can minimize these oscillations.

PACS numbers: 72.20.Pa, 73.21.La, 71.15.Mb

## I. INTRODUCTION

Single electron devices made up of a confined nanostructure located in the vicinity of electrodes that act as electron baths constitute a viable alternative to traditional field effect transistors which are about to reach their physical minimum size in a few years<sup>1</sup>. Therefore, detailed study of these devices has accelerated recently aided by the tremendous advances in nanotechnology during the past two decades. To this end, it is of critical importance to simulate the switching characteristics of these prototypes in the presence of realistic electron-electron and electron-phonon interactions to assess their suitability for large electrical circuits.

Early studies largely focused on the influence of the many-body Kondo resonance on the transient electrical conductance and discovered that various time scales<sup>2,3</sup> emerge after sudden switching of the gate or bias voltage<sup>4-6</sup>. These timescales are inherently related to the spin fluctuations that govern the amount of time required for full formation of the Kondo resonance<sup>4</sup>. Moreover, it turns out that the Van Hove singularities in the electrode density of states can induce dramatic effects in transient conductance. Damped oscillations arising from interference between the emerging Kondo resonance and the singularities in the contact density of states have been initially reported using prototypical density of states for an asymmetrically coupled system<sup>7</sup>. Subsequent studies undertaken to make the theoretical predictions more realistic used the electrode density of states calculated via ab initio methods as an input in many body calculations and exposed beating phenomena in transient electrical

conductance<sup>8,9</sup>.

Kondo effect is probably the most elegant and exotic example of many body physics whose signature has been originally traced in magnetic impurities embedded in bulk metals as resistance enhancement at low temperatures<sup>24</sup>. It took some four decades to unravel its existence in confined nanostructures like quantum dots<sup>25</sup> and molecules<sup>26,27</sup>. The underlying physical mechanism for the Kondo effect is the spin flip processes taking place at low temperatures between an isolated spin at dot energy level and the Fermi sea of electrons at electrodes. When the dot energy level lies below the Fermi level, a sharp resonance develops around the Fermi level and it causes an enhancement in current due to the opening of an extra transport channel. The linewidth of this resonance is on the order of an energy scale called the Kondo temperature  $T_K$  given by

$$T_K \approx \left( \frac{D\Gamma_{tot}}{4} \right)^{\frac{1}{2}} \exp \left( -\frac{\pi|\epsilon_{dot}|}{\Gamma_{tot}} \right), \quad (1)$$

where  $D$  is the half bandwidth of the conduction electrons and  $\Gamma_{tot}$  is the total coupling of the dot to the electrodes. In this paper, we will take  $D = 9\Gamma_{tot}$ .

Introducing a temperature gradient across the electrodes provides another intriguing and realistic path for investigation. The existence of Kondo resonance can be checked directly via a measurement of the thermopower (Seebeck coefficient)  $S$  and the thermoelectric figure of merit  $ZT$  which is directly related to the thermopower is a key indicator of the device's performance. Some experiments in molecular junctions have recently probed this by adjusting the alignment of the impurity orbital with re-

spect to the Fermi level of the contacts and this has been found to result in a change of sign in thermopower<sup>10–13</sup>.

Behaviour of the thermopower and figure of merit has been elucidated as a function of temperature both in Kondo<sup>14–16</sup> and mixed valence regimes<sup>16</sup>. These studies were largely in line with the experimental work and confirmed the critical role the impurity energy level plays in the sign of thermopower. Nevertheless, they were by no means sufficient to shed light on the thermal switching behaviour of these devices since they were performed in steady state. Thermal switching will be required in practical applications to be able to operate the device at different thermoelectric figure of merit values. Therefore, it is imperative to understand the behaviour of the thermal switch in transient region. First analysis of the thermopower in a time-dependent situation showed that the the inverse of the saturated decay time of thermopower to its steady state value is equal to the Kondo temperature when Kondo resonance emerges as a result of the sudden motion of the dot level to a position nearby the Fermi level of the electrodes<sup>17</sup>. Later, ac driving of the dot level sinusoidally revealed complex fluctuations in instantaneous thermopower whose extreme values are quite sensitive to the amplitude of the oscillation<sup>18</sup>.

These studies utilized parabolic density of states for contacts and the effect of singularities on the instantaneous thermopower and figure of merit in Kondo regime remains to be seen. It is our aim in this paper to fill this gap and investigate the behaviour of instantaneous thermopower and figure of merit for a quantum dot whose energy level is shifted to a position close to the Fermi level of contacts. This gives rise to the gradual appearance of the Kondo resonance slightly above the Fermi level.

## II. THEORY

We will assume that the quantum dot energy levels are filled completely until its highest occupied molecular (HOMO) level with two electrons of opposite spins. We will represent the HOMO level with a single discrete spin degenerate energy level  $\varepsilon_{dot}$  coupled to electrodes which are free electron baths. This physical system can be mapped to the Anderson hamiltonian which can be written as

$$H(t) = \sum_{\sigma} \varepsilon_{dot}(t) n_{\sigma} + \sum_{k\alpha\sigma} \varepsilon_k n_{k\alpha\sigma} + \frac{1}{2} \sum_{\sigma,\sigma'} U_{\sigma,\sigma'} n_{\sigma} n_{\sigma'} + \sum_{k\alpha\sigma} \left[ V_{\alpha}(\varepsilon_{k\alpha}, t) c_{k\alpha\sigma}^{\dagger} c_{\sigma} + \text{H.c.} \right], \quad (2)$$

where  $c_{\sigma}^{\dagger}$  ( $c_{\sigma}$ ) and  $c_{k\alpha\sigma}^{\dagger}$  ( $c_{k\alpha\sigma}$ ) with  $\alpha=L,R$  create (destroy) an electron of spin  $\sigma$  in the dot energy level and in the left(L) and right(R) electrodes respectively. The  $n_{\sigma}$  and  $n_{k\alpha\sigma}$  are occupancies of the dot energy level and the electrode  $\alpha$ .  $V_{\alpha}$  are the tunneling amplitudes between the electrode  $\alpha$  and the quantum dot. This model is an ideal

venue to study Kondo correlations since it can be mapped directly to Kondo model via Schrieffer-Wolf transformations. The Coulomb repulsion energy  $U$  in this model represents the charging energy of the dot. This corresponds to the energy gap between the HOMO level and the lowest unoccupied molecular (LUMO) level. We take the charging energy to be infinite. This is in line with the experiments which indicate that the typical charging energy of quantum dots overwhelm the other tunable parameters in the Kondo regime. This choice results in single occupancy of the dot energy level with up or down spin. Moreover, we will be using atomic units where we take  $\hbar = k_B = e = 1$ .

We redefine the electron operators on the dot by introducing a massless (slave) boson operator and a pseudofermion operator<sup>19</sup> as

$$c_{\sigma} = b^{\dagger} f_{\sigma}. \quad (3)$$

These new operators must also satisfy

$$Q = b^{\dagger} b + \sum_{\sigma} f_{\sigma}^{\dagger} f_{\sigma} = 1. \quad (4)$$

which ensures one to one mapping between the Anderson hamiltonian and the transformed hamiltonian in  $U \rightarrow \infty$  limit by limiting the dot energy level occupancy to single electron. We can safely omit the Hubbard term from the transformed Hamiltonian which turns out to be

$$H(t) = \sum_{\sigma} \varepsilon_{dot}(t) n_{\sigma} + \sum_{k\alpha\sigma} \left[ \varepsilon_k n_{k\alpha\sigma} + V_{\alpha}(\varepsilon_{k\alpha}, t) c_{k\alpha\sigma}^{\dagger} b^{\dagger} f_{\sigma} + \text{H.c.} \right], \quad (5)$$

where  $f_{\sigma}^{\dagger}$  ( $f_{\sigma}$ ) and  $b^{\dagger}$  ( $b$ ) with  $\alpha=L,R$  are creation(destruction) operators for an electron with spin  $\sigma$  and a slave boson on the dot energy level.

Taking time independent hopping matrix elements, the total coupling of the quantum dot to the electrodes is given by  $\Gamma_{L(R)}(\epsilon) = \bar{\Gamma}_{L(R)} \rho_{L(R)}(\epsilon)$ , where  $\bar{\Gamma}_{L(R)}$  is a constant given by  $\bar{\Gamma}_{L(R)} = 2\pi |V_{L(R)}(\epsilon_f)|^2$  and  $\rho_{L(R)}(\epsilon)$  is the density of states function of the electrodes. Both left and right electrodes are taken to be made up of the same material in conjunction with experiments implying that  $\rho_L(\epsilon) = \rho_R(\epsilon) = \rho(\epsilon)$ . Consequently, we obtain  $\Gamma_{tot}(\epsilon) = \bar{\Gamma}_{tot} \rho(\epsilon)$  where  $\Gamma_{tot}(\epsilon) = \Gamma_L(\epsilon) + \Gamma_R(\epsilon)$  and  $\bar{\Gamma}_{tot} = \bar{\Gamma}_L + \bar{\Gamma}_R$ .

Graphene is a highly resilient and versatile material which has been manufactured in large quantities quite recently thanks to the scotch tape method<sup>20</sup>. Its unique features largely stem from the fact that it can be considered both a semiconductor with zero bandgap and a metal whose density of states is zero at the Fermi level<sup>21</sup>. The first type of contact we choose in Fig. 1 mimics the density of states of graphene  $\rho(\epsilon)$  except that we added an infinitesimal thick cylindrical feature inside the conic structure which results in nonzero value at the Fermi level to enable the proper development of the Kondo resonance. In this case, the Van Hove singularity lies at

the bottom of the band. Since we assume that the dot is weakly coupled to the electrodes, the band cutoff at  $D = 9\Gamma_{tot}$  lies at a sufficiently low energy. This enables us to safely ignore deviations from the linear dispersion relation at high energies and the Dirac cone approximation is still valid. The second type of contact depicted in Fig. 1 is a prototypical metal and of triangular shape. Once again we added a cylindrical feature with infinitesimal thickness inside the triangle to enable nonzero value at the Fermi level. The Van Hove singularity lies in the middle of the band in this latter case.

In both cases, we showed only the valence bands in Fig. 1 for simplicity. The conduction bands are just the mirror image of valence bands across the Fermi level. Furthermore, we made sure the number of electrons is the same in both cases by integrating the area from the bottom of the band to the top. The latter one is a necessary step to facilitate direct comparison between the two structures. In particular, the density of states function for graphene in Fig. 1a is given by

$$\begin{aligned} \rho(\epsilon) &= 2.17 |\epsilon| + \delta \text{ if } |\epsilon| \leq D \\ \rho(\epsilon) &= 0 \text{ if } |\epsilon| > D, \end{aligned} \quad (6)$$

where the prefactor corresponds to the inverse of the Fermi velocity in atomic units and  $\delta$  is an infinitesimal number. On the other hand, the density of states function for the metal shown in Fig. 1b is

$$\begin{aligned} \rho(\epsilon) &= 4.34 |\epsilon| + \delta \text{ if } |\epsilon| \leq 0.5D \\ \rho(\epsilon) &= -4.34 |\epsilon| + \delta + 4.34D \text{ if } 0.5D \leq |\epsilon| \leq D \\ \rho(\epsilon) &= 0 \text{ if } |\epsilon| > D. \end{aligned} \quad (7)$$

Our technique to tackle the slave boson Hamiltonian in Eq. (5) relies on the double time Kadanoff-Baym Green functions which have been adapted to the quantum impurity problems<sup>22,23</sup>. In particular, the retarded Green function is given by

$$G^R(t, t_1) = -i\theta(t - t_1) < \{c_\sigma(t), c_\sigma^\dagger(t_1)\} >, \quad (8)$$

where the curly brackets denote anticommutation. After performing the slave boson transformation described above, the retarded Green function can be redefined in terms of the slave boson and pseudofermion Green functions<sup>7</sup> as

$$\begin{aligned} G^R(t, t_1) &= -i\theta(t - t_1) [G_{pseudo}^R(t, t_1) B^<(t_1, t) \\ &\quad + G_{pseudo}^<(t, t_1) B^R(t_1, t)]. \end{aligned} \quad (9)$$

The task then boils down to calculating these double time Green functions. We handle this by solving coupled Dyson equations in a two-dimensional cartesian grid whose dimensions correspond to the time arguments of the Green function. Care must be taken in this procedure to build the memory effect into the calculation. This is accomplished by performing a convergence test via increasing size of the matrix in which the values of the Green function are stored.

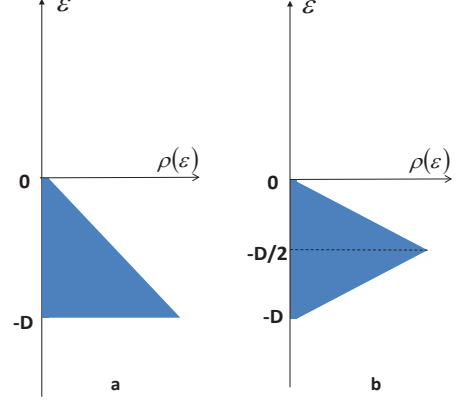


FIG. 1: This figure illustrates the density of states function  $\rho(\epsilon)$  of contacts to which the quantum dot is attached. Since both left and right electrodes are identical, only one of them is shown.

In order to solve the coupled Dyson equations, the pseudofermion and slave boson self energies must be approximated somehow since they are critical inputs to these equations. We omit higher order corrections and thus are content with the non-crossing approximation(NCA)<sup>3,23</sup> for this purpose. As crude as it looks, it is known to give remarkably correct results for dynamical quantities at zero magnetic field outside the Fermi liquid regime which corresponds to temperatures much smaller than the Kondo energy scale. We will stay away from the Fermi liquid regime in this paper for this reason. Once the Green functions are obtained in this method, the matrix that stores their values is propagated in time in discrete steps diagonally. This is how the instantaneous values of the physical quantities are determined.

The physical quantities we will be interested are electrical conductance  $G(t)$ , thermal conductance  $\kappa(t)$  and thermopower  $S(t)$ . In linear response, their instantaneous values can be expressed in terms of the Onsager coefficients given by

$$\begin{aligned} L_{11}(t) &= T \times \\ &\quad \text{Im} \left( \int_{-\infty}^t dt_1 \int \frac{d\epsilon}{2\pi} e^{i\epsilon(t-t_1)} \Gamma_{tot}(\epsilon) G^r(t, t_1) \frac{\partial f(\epsilon)}{\partial \epsilon} \right), \\ L_{12}(t) &= T^2 \times \\ &\quad \text{Im} \left( \int_{-\infty}^t dt_1 \int \frac{d\epsilon}{2\pi} e^{i\epsilon(t-t_1)} \Gamma_{tot}(\epsilon) G^r(t, t_1) \frac{\partial f(\epsilon)}{\partial T} \right), \\ L_{22}(t) &= T^2 \times \\ &\quad \text{Im} \left( \int_{-\infty}^t dt_1 \int \frac{d\epsilon}{2\pi} e^{i\epsilon(t-t_1)} \Gamma_{tot}(\epsilon) \epsilon G^r(t, t_1) \frac{\partial f(\epsilon)}{\partial T} \right) \end{aligned}$$

where  $f(\epsilon)$  is the Fermi-Dirac distribution function given by  $f(\epsilon) = \frac{1}{1+e^{\beta\epsilon}}$  with  $\beta = \frac{1}{T}$ .

In terms of these coefficients, the physical quantities can be cast as

$$\begin{aligned} G(t) &= \frac{L_{11}(t)}{T}, \\ \kappa(t) &= \frac{1}{T^2} \left( L_{22}(t) - \frac{L_{12}^2(t)}{L_{11}(t)} \right), \\ S(t) &= \frac{L_{12}(t)}{TL_{11}(t)}. \end{aligned} \quad (11)$$

On the other hand, the figure of merit of a nanodevice is a dimensionless quantity which is an indicator of its efficiency. Hence, it is a benchmark on its performance in a circuit. In terms of the previously defined quantities, it is given by

$$ZT = \frac{S^2(t)G(t)T}{\kappa(t)}. \quad (12)$$

The figure of merit always acquires a positive value and larger figure of merit values imply better performance. We will be ignoring the phonon contribution to the thermal conductance. This assumption is justified because we will be carrying out our calculations around the Kondo temperature of the device which is only a few Kelvins. Phonon contribution to the thermal conductance can be safely ignored in this regime compared to the electronic one in contrast with some previous work where the system is outside Kondo regime and the ambient temperature is several hundred Kelvins<sup>28,29</sup>.

In this paper, we will be concerned with the behaviour of instantaneous thermopower and figure of merit for a quantum dot whose energy level is shifted suddenly to a position close to Fermi levels of contacts such that the Kondo resonance can develop in this final state. We will have the chance to make a direct comparison between the effect of metal and graphene type electrodes on transient values of these quantities. This constitutes a fairly realistic model to simulate the thermal switching behaviour of single electron devices since electron-electron interactions are captured as well as the structure of the electrode material. Hence, our investigation should shed light on design and implementation of these devices experimentally. Our only limitation will be that our results will pertain to linear response only due to the validity of Onsager coefficients in this regime. This is also realistic because infinitesimal temperature gradient between the electrodes can be achieved easily by illuminating one of the contacts with a faint laser beam.

### III. RESULTS AND DISCUSSION

In this section, we will present our numerical results on the instantaneous thermopower and figure of merit of a single quantum dot whose energy level is abruptly moved from  $\epsilon_{dot} = -5\Gamma_{tot}$  to  $\epsilon_{dot} = -2\Gamma_{tot}$  via a gate voltage. This motion triggers a transition from a state where the Kondo resonance is completely absent to a state where

the Kondo resonance gradually emerges. This transition takes place due to a drastic change in Kondo temperature  $T_K$  since it critically depends on the position of the dot energy level  $\epsilon_{dot}$  as seen in Eq. (1).

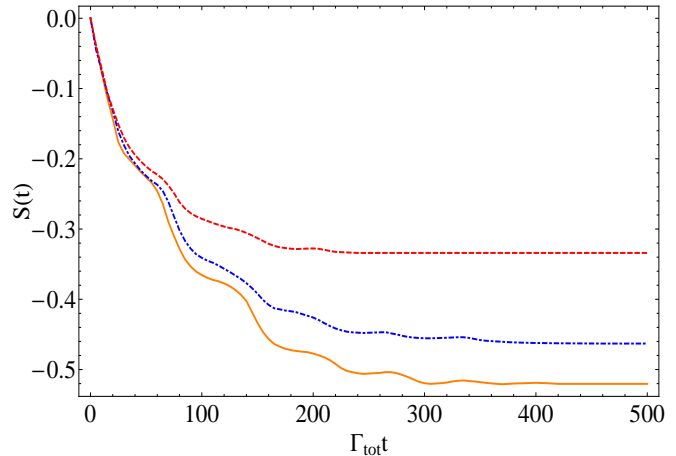


FIG. 2: This figure shows the instantaneous thermopower  $S(t)$  immediately after the dot energy level has been moved to its final position for ambient temperatures of  $0.0035\Gamma_{tot}$  (red dashed),  $0.0028\Gamma_{tot}$  (blue dot dashed) and  $0.0014\Gamma_{tot}$  (orange solid) in linear response for metal electrodes shown in Fig. 1b.

We will start our analysis with the instantaneous thermopower results. Fig. 2 depicts the instantaneous thermopower for three different ambient temperatures immediately after the dot level has been switched to its final location for metal electrodes shown in Fig. 1b. The Kondo temperature in the final state is inferred to be  $T_K = 0.0021\Gamma_{tot}$ . Consequently, the higher two temperatures are above  $T_K$  while the lowest temperature is slightly lower. We see in this figure that damped sinusoidal oscillations start developing at the onset of Kondo timescale with the same frequency for all temperatures.

Kondo timescale, during which the Kondo resonance starts emerging slightly above the Fermi level, takes place after the short timescale which corresponds to charge fluctuations. Short timescale roughly takes place between  $0 < \Gamma_{tot}t < 10$ . This result is quite interesting and different from conductance oscillations which appear much later at  $\Gamma_{tot}t > 80^2$ . Another novelty is the insensitivity of these oscillations to asymmetry of the junction defined as  $\eta = \bar{\Gamma}_L/\bar{\Gamma}_{tot}$ . Changing the asymmetry factor  $\eta$  does not effect the frequency and amplitude of the oscillations. Moreover, the final steady state thermopower (i.e.  $\Gamma_{tot}t \rightarrow \infty$ ) also remains unchanged when  $\eta$  is altered in conjunction with other studies investigating steady state thermopower<sup>30</sup>. The only resemblance these results bear to instantaneous conductance data is the saturation of the amplitudes below the Kondo temperature. We did not show the curves well below  $T_K$  in Fig. 2 as they overlap with higher temperature ones and obscure the oscillations. The oscillation frequency is the same at all temperatures and the oscillations persist deep into the long timescale with  $\Gamma_{tot}t > 300$  when  $T \leq T_K$ .

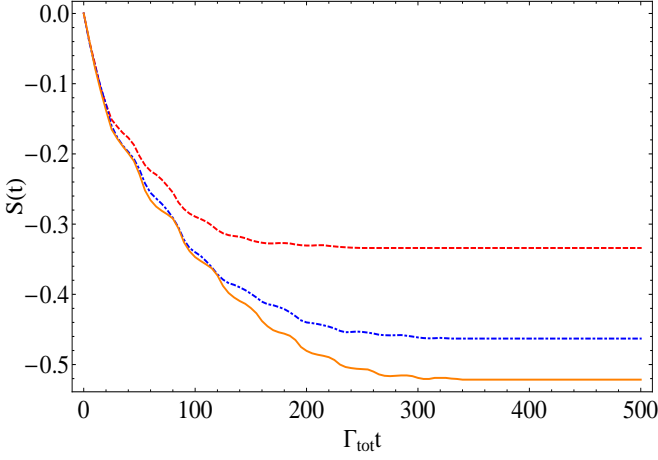


FIG. 3: This figure shows the instantaneous thermopower  $S(t)$  immediately after the dot energy level has been moved to its final position for ambient temperatures of  $0.0035\Gamma_{tot}$  (red dashed),  $0.0028\Gamma_{tot}$  (blue dot dashed) and  $0.0014\Gamma_{tot}$  (orange solid) in linear response for graphene electrodes shown in Fig. 1a.

Fig. 3 displays our numerical results for the instantaneous thermopower using the same parameters used in Fig. 2. The major difference is that the quantum dot is attached to graphene electrodes shown in Fig. 1a. The oscillations starting in the Kondo timescale are still present here. However, their amplitudes are suppressed dramatically compared to metal electrodes. On the other hand, the steady state thermopower values are still the same as Fig. 2 but the oscillation frequency doubled. These results obviously suggest that graphene is a more desirable material to be used as electrode in single electron devices because it enables to minimize if not completely suppress the undesirable fluctuations during the switching of these devices. This is a great advantage in integrating these devices into larger circuits.

We want to dwell on the underlying microscopic mechanism for these oscillations. The numerical results presented above show that the frequency of oscillations is proportional to the energy separation between the Fermi level of the contacts and the sharp feature in the density of states of the contacts. That feature happens to be in the edge of the band for graphene therefore it generates the highest frequency. More importantly, the amplitude of the oscillations decreases as the energy separation between the Fermi level and the sharp feature increases resulting in the minimum amplitude for graphene.

In order to generalize and verify this conclusion, we performed additional calculations with the same parameters in Fig. 2 and Fig. 3 by using metal electrodes whose density of states is triangular like Fig. 1b except the fact that the van Hove singularity is located at  $-0.75D$ . We calculated the amplitude of the nearest peak or trough occurring around  $\Gamma_{tot}t=200$  for all three electrodes. The amplitude has been determined by taking the average of the two amplitudes corresponding to the two adjacent

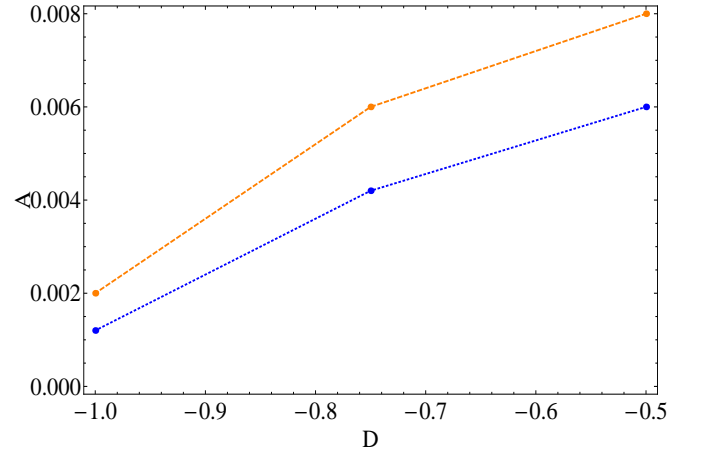


FIG. 4: This figure shows the amplitude of the peak or trough nearest to  $\Gamma_{tot}t=200$  that occurs in thermopower oscillations at ambient temperature of  $0.0014\Gamma_{tot}$  (orange dashed) and  $0.0028\Gamma_{tot}$  (blue dotted) as a function of the position of the van Hove singularity in the contact density of states. Solid dots represent the actual data points.

peak-trough pairs. This step is necessary because the oscillations are damped. The results are shown in Fig. 4 for two ambient temperatures as a function of the position of the van Hove singularity and it is obvious from here that the graphene electrodes where the van Hove singularity is at  $-D$  produce minimum amplitude at both temperatures. The instant  $\Gamma_{tot}t=200$  is arbitrary and same calculation at other instants yields similar results. If the dot gets attached to electrodes made up of two dimensional electron gas with flat density of states and the same bandwidth  $D$ , the oscillation frequency is the same as graphene because the van Hove singularity still lies at the edge of the band. However, the oscillation amplitudes turn out to be larger than graphene presumably due to the large difference in the value of the density of states at Fermi level.

These results suggest the presence of an interference process. The components of this interference should be the two sharp features. These are nothing but the van Hove singularity in the density of states of the electrodes and the Kondo resonance in the dot density of states. This interference is enabled due to two factors. First, the density of states of the dot and the electrodes are mixed due to the hybridization term in the Hamiltonian therefore the Kondo resonance and the van Hove singularity can interact even though they are not located in the same density of states. Second, the development of the Kondo resonance is gradual and it is fully formed only at the end of the long timescale<sup>2</sup> implying that it is a dynamical time-dependent feature. On the other hand, the van Hove singularity at the contact density of states is static and it does not evolve in time. Consequently, the interference can take place between a dynamic and a static feature. It dies out once they both become static, hence we observe damped oscillations.

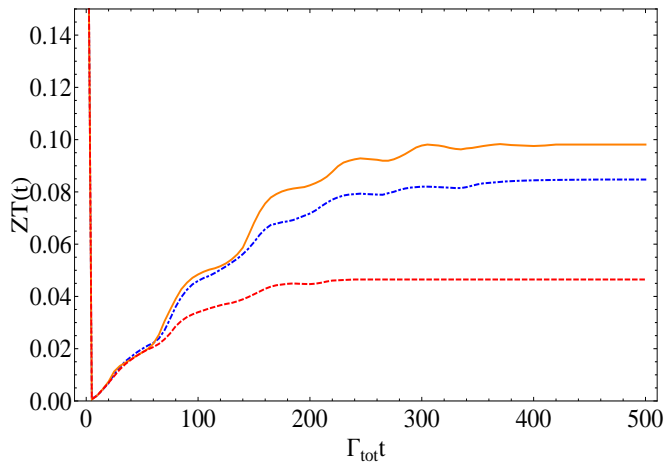


FIG. 5: This figure shows the instantaneous figure of merit  $ZT(t)$  immediately after the dot energy level has been moved to its final position for ambient temperatures of  $0.0035\Gamma_{tot}$  (red dashed),  $0.0028\Gamma_{tot}$  (blue dot dashed) and  $0.0014\Gamma_{tot}$  (orange solid) in linear response for metal electrodes shown in Fig. 1b.

The thermopower is related to the dot density of states at low temperatures via Sommerfeld expansion which is given by

$$S(T) = -\frac{\pi^2 T}{3A(0, T)} \frac{\partial A}{\partial \epsilon} \Big|_{\epsilon=0} \quad (13)$$

in atomic units.  $A(0, T)$  corresponds to the value of the dot density of states at Fermi level of the contacts and  $\frac{\partial A}{\partial \epsilon}$  is its derivative. The formation of the Kondo resonance has been previously shown to take place slightly above the Fermi level<sup>31</sup> giving rise to a positive derivative at Fermi level. Consequently, the overall sign of the thermopower in the final state is always negative. As the Kondo resonance starts growing in the final state, the derivative begins to increase in magnitude. When the Kondo resonance reaches its full form in the long timescale, the derivative stabilizes. This causes the thermopower to reach its steady state.

The fundamental difference between the oscillations in the thermopower and the conductance reported previously lies in their start of occurrence and sensitivity to asymmetry. The thermopower oscillations start much earlier than the conductance oscillations because tiny fluctuations in the dot density of states at Fermi level due to this interference are enhanced as a result of the derivative in Sommerfeld expansion and thus manifest themselves in the thermopower at the onset of Kondo timescale prominently. The insensitivity to asymmetry originates from the constructive interference of the right and left electrodes with the Kondo resonance magnifying the effect even further. The destructive interference between the left and right electrodes diminishes the conductance oscillations gradually with increasing  $\eta^{7-9}$ .

We also want to go over the instantaneous figure of merit results. We use the same parameters in Fig. 2 and

Fig. 3 for this purpose. Fig. 5 displays the instantaneous figure of merit immediately after the dot level has been switched to its final position for metal electrodes. A first glance at this figure reveals that the figure of merit is nonzero in initial state on contrary to the thermopower shown in Fig. 2 and Fig. 3. This can be understood by simplifying the figure of merit using the Wiedemann-Franz law. The ratio of the thermal conductivity to electrical conductivity is given by the Wiedemann-Franz law which can be expressed as

$$\frac{\kappa(t)}{G(t)} = LT, \quad (14)$$

where  $L$  is a constant called the Lorentz number. It can be cast as  $L = \pi^2/3$  in atomic units. Inserting this identity into Eq. (12) gives

$$ZT = S^2(t)/L. \quad (15)$$

This obviously implies that the thermoelectric figure of merit can never be negative and is proportional to the square of the instantaneous thermopower which we just investigated. However, the main subtlety is that the value of the Lorentz number deviates from its real value in mesoscopic systems including quantum dots outside the Fermi liquid state. Fermi liquid state occurs when  $T \ll T_K$ . Incidentally, our calculations invoking NCA is valid outside the Fermi liquid state too. In the initial dot energy level,  $T \gg T_K$  and our numerical results reveal a much larger thermoelectric figure of merit than the final dot energy level owing to the suppression of the Lorentz number greatly in line with previous steady state results<sup>14-16</sup>. Consequently, the instantaneous figure of merit exhibits a sharp jump upon switching the dot level abruptly at  $t=0$ .

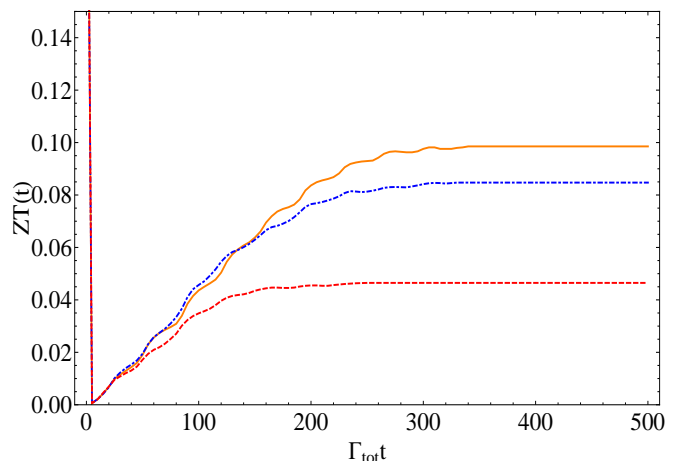


FIG. 6: This figure shows the instantaneous figure of merit  $ZT(t)$  immediately after the dot energy level has been moved to its final position for ambient temperatures of  $0.0035\Gamma_{tot}$  (red dashed),  $0.0028\Gamma_{tot}$  (blue dot dashed) and  $0.0014\Gamma_{tot}$  (orange solid) in linear response for graphene electrodes shown in Fig. 1a.



The behaviour of the instantaneous figure of merit curves in the final state generally follows the square of the respective instantaneous thermopower curves. The oscillation frequency is again the same in this case. Besides these obvious points, there is a much more intricate issue that is worth pointing out here. We deliberately chose ambient temperatures that are around  $T_K$  for our calculations. An earlier investigation showed that the value of the Lorentz number declines with a sharp slope upon passing through  $T_K$  as a function of temperature<sup>15</sup>. This rapid change of the value of the Lorentz number plays an important role for our time dependent calculations. This role stems from the fact that the instantaneous figure of merit is proportional to the inverse of the Lorentz number as seen in Eq. (15).

The  $1/L$  serves as an enhancement factor for the instantaneous figure of merit. The amplitudes of the oscillations taking place at or above the Kondo temperature  $T_K$  are enhanced more than the amplitudes of the oscillations occurring at ambient temperatures below  $T_K$  as a result of this slope around  $T_K$ . This can be seen in Fig. 5. On the other hand, Fig. 6 shows the instantaneous figure of merit results for the same parameters used in Fig. 5 when the quantum dot is attached to graphene electrodes. We see in this figure that the graphene electrodes largely suppress the amplitude of the oscillations compared to Fig. 5 due to the larger energy gap between the Van Hove singularity at the edge of the band and the Fermi level. This also doubles the oscillation frequency compared to Fig. 5. Main advantage of this suppression is the prevention of the sudden drop of the device performance at trough points.

Another interesting peculiarity occurring in Fig. 6 due to the sharp variation of the value of the Lorentz number across  $T_K$  is that the value of the instantaneous thermopower at an ambient temperature above  $T_K$  can temporarily exceed the value of the instantaneous thermopower below  $T_K$ . This can be seen between  $40 < \Gamma_{tot}t < 140$ . This is clearly a transient phenomena and cannot be accessed with a steady-state formalism.

#### IV. CONCLUSIONS

In conclusion, we studied in linear response both the instantaneous thermopower and figure of merit for a quantum dot whose energy level is suddenly moved into a position such that the many body Kondo resonance develops in the final position. We modeled graphene and metal type contacts for this purpose. We uncov-

ered damped sinusoidal oscillations starting at the onset of the Kondo timescale and persisting until the long timescale regardless of the asymmetry factor. This behaviour is distinct and different from the instantaneous conductance oscillations which were investigated previously in great detail. The frequency of these oscillations turns out to be proportional to the separation between the Fermi level of the contacts and the van Hove singularity in the contact density of states. The amplitudes more or less saturate around the Kondo timescale suggesting that the interference between the Kondo resonance and the van Hove singularities is the underlying physical mechanism for these oscillations. This interference gives rise to small fluctuations in the dot density of states at Fermi level whose effects are amplified in the thermopower through its derivative in the Sommerfeld expansion. This results in fairly large oscillation amplitudes for metallic electrodes. However, graphene contacts generate the smallest amplitude since their van Hove singularity lies farthest away from the Fermi level minimizing the interference. This renders graphene as an ideal electrode candidate for future single electron devices.

We also investigated the instantaneous figure of merit for the same set up. Violation of the Wiedeman-Franz law causes peculiarities here. A sharp decline of the value of the Lorentz number around the Kondo temperature results in an enhancement of the oscillations above the Kondo temperature more than the ones occurring below the Kondo temperature. Due to this subtlety, the value of the instantaneous thermopower at an ambient temperature above  $T_K$  can temporarily exceed the value of the instantaneous thermopower below  $T_K$  in the Kondo timescale.

As a final note, we would like to comment on the experimental feasibility of our work. Graphene sheets can be manufactured routinely via scotch tape method and quantum dots are produced via molecular beam epitaxy quite easily. The small temperature gradient between the contacts can be obtained by illuminating one of the contacts with a faint laser beam. Moreover, recent remarkable progress in ultrafast pump-probe methods<sup>32,33</sup> should make measuring thermopower and thermal conductance in real time possible.

#### V. ACKNOWLEDGMENTS

The authors thank Tübitak for generous financial support via grant 111T303.

<sup>1</sup> Likharev K K 2003 in J Greer, A Korkin and J Labanowski, eds, *Nano and Giga challenges in microelectronics* (Dordrecht: Elsevier) pp 27–68

<sup>2</sup> Plihal M, Langreth D C and Nordlander P 2005 *Phys. Rev. B* **71** 165321

<sup>3</sup> Izmaylov A F, Goker A, Friedman B A and Nordlander P 2006 *J. Phys.: Condens. Matter* **18** 8995–9006

<sup>4</sup> Nordlander P, Pustilnik M, Meir Y, Wingreen N S and Langreth D C 1999 *Phys. Rev. Lett.* **83** 808–811

<sup>5</sup> Plihal M, Langreth D C and Nordlander P 2000 *Phys. Rev.*

- B* **61** R13341–13344
- <sup>6</sup> Merino J and Marston J B 2004 *Phys. Rev. B* **69** 115304
  - <sup>7</sup> Goker A, Friedman B A and Nordlander P 2007 *J. Phys.: Condens. Matter* **19** 376206
  - <sup>8</sup> Goker A, Zhu Z Y, Manchon A and Schwingenschlogl U 2010 *Phys. Rev. B* **82** 161304(R)
  - <sup>9</sup> Goker A, Zhu Z Y, Manchon A and Schwingenschlogl U 2011 *Chem. Phys. Lett.* **509** 48
  - <sup>10</sup> Reddy P, Jang S Y, Segalman R A and Majumdar A 2007 *Science* **315** 1568
  - <sup>11</sup> Baheti K, Malen J A, Doak P, Reddy P, Jang S Y, Tilley T D, Majumdar A and Segalman R A 2008 *Nano Lett.* **8** 715
  - <sup>12</sup> Malen J A, Doak P, Baheti K, Tilley T D, Majumdar A and Segalman R A 2009 *Nano Lett.* **9** 3406
  - <sup>13</sup> Tan A, Sadat S and Reddy P 2010 *Appl. Phys. Lett.* **96** 13110
  - <sup>14</sup> Yang K H, Zhao Y L, Wu Y J and Wu Y P 2010 *Phys. Lett. A* **374** 2874
  - <sup>15</sup> Dong B and Lei X L 2002 *J. Phys.:Condens. Matter* **14** 11747
  - <sup>16</sup> Costi T A and Zlatic V 2010 *Phys. Rev. B* **81** 235127
  - <sup>17</sup> Goker A and Uyanik B 2012 *Phys. Lett. A* **376** 2735
  - <sup>18</sup> Goker A and Gedik E 2013 *J. Phys.:Condens. Matter* **25** 125301
  - <sup>19</sup> Coleman P 1984 *Phys. Rev. B* **29** 3035
  - <sup>20</sup> Geim A K and Novoselov K S 2007 *Nature Materials* **6** 183–191
  - <sup>21</sup> Neto A A C, Guinea F, Peres N M R, Novoselov K S and Geim A K 2009 *Rev. Mod. Phys.* **81** 109–162
  - <sup>22</sup> Langreth D C and Nordlander P 1991 *Phys. Rev. B* **43** 2541–2557
  - <sup>23</sup> Shao H X, Langreth D C and Nordlander P 1994 *Phys. Rev. B* **49** 13929–13947
  - <sup>24</sup> Kondo J 1964 *Prog. Theor. Phys.* **32** 37
  - <sup>25</sup> Goldhaber-Gordon D, Shtrikman H, Mahalu D, Abusch-Magder D, Meirav U and Kastner M A 1998 *Nature* **391** 156–159
  - <sup>26</sup> Liang W J, Shores M P, Bockrath M, Long J R and Park H 2002 *Nature* **417** 725
  - <sup>27</sup> Park J, Pasupathy A N, Goldsmith J I, Chang C, Yaish Y, Petta J R, Rinkoski M, Sethna J P, Abruna H D, McEuen P L and Ralph D C 2002 *Nature* **417** 722
  - <sup>28</sup> Bergfield J P, Solis M A and Marston J B 2010 *ACS Nano* **4** 5314
  - <sup>29</sup> Tsaousidou M and Triberis G P 2010 *J. Phys.: Condens. Matter* **22** 355304
  - <sup>30</sup> Krawiec M and Wysokinski K I 2007 *Phys. Rev. B* **75** 155330
  - <sup>31</sup> Costi T A, Hewson A C and Zlatic V 1994 *J. Phys.:Condens. Matter* **6** 2519
  - <sup>32</sup> Terada Y, Yoshida S, Takeuchi O and Shigekawa H 2010 *J. Phys.: Condens. Matter* **22** 264008
  - <sup>33</sup> Terada Y, Yoshida S, Takeuchi O and Shigekawa H 2010 *Nat. Photon.* **4** 869